

Earthquake magnitude with DAS: a transferable data-based scaling relation

Jiuxun Yin¹, Weiqiang Zhu¹, Jiaxuan Li¹, Ettore Biondi¹, Yaolin Miao², Zack
J. Spica², Loïc Viens³, Masanao Shinohara⁴, Satoshi Ide⁵, Kimihiro
Mochizuki⁴, Allen L. Husker¹, Zhongwen Zhan¹

¹Seismological Laboratory, Division of Geological and Planetary Sciences, California Institute of
Technology, Pasadena, CA, USA

²Department of Earth and Environmental Sciences, University of Michigan, Ann Arbor, MI, USA

³Los Alamos National Laboratory, Los Alamos, New Mexico, USA

⁴Earthquake Research Institute, University of Tokyo, Yayoi 1-1-1, Bunkyo-ku, Tokyo, 113-0032, Japan

⁵Department of Earth and Planetary Science, University of Tokyo, Hongo 7-3-1, Bunkyo-ku, Tokyo,
113-0033, Japan

Key Points:

- We present the first data-based scaling relation for the DAS amplitude of earthquakes.
- Earthquake magnitude can be accurately estimated from DAS amplitude with the scaling relation.
- The DAS scaling relation is transferable and can be transferred from one area to another new area.

Corresponding author: Jiuxun Yin, yinjax@caltech.edu

Abstract

Distributed Acoustic Sensing (DAS) is a promising technique to improve the rapid detection and characterization of earthquakes. Due to some instrumental limitations, current DAS studies primarily focus on the phase information but less on the amplitude information. In this study, we compile earthquake data from two DAS arrays in California, USA, and one submarine array in Sanriku, Japan. We develop a data-driven method to obtain the first scaling relation between DAS amplitude and earthquake magnitude. Our results reveal that the DAS amplitude in different regions follows a similar scaling relation. The scaling relation can provide a rapid magnitude estimation and effectively avoid uncertainties caused by the conversion to ground motions. We finally show that the scaling relation is transferable from one to another new region. The scaling relation highlights the great potential of DAS in earthquake source characterization and early warning.

Plain Language Summary

Distributed Acoustic Sensing (DAS) is an emerging technique that can convert an optical fiber cable into a dense array to record clear earthquake signals. The recorded signals have essential information about earthquakes. For example, DAS can record higher amplitude signals from earthquakes with larger magnitude. However, conditions of the optical cables, such as how they are installed or how well they are attached to the surrounding medium, are often unknown, thus preventing quantitative measuring of earthquake magnitude from the DAS measurement. In this study, we investigate the earthquake data recorded by different DAS arrays and develop a data-driven method to get an empirical relation between the earthquake magnitude and the amplitude of DAS signals. We show that this empirical relation can accurately estimate the earthquake magnitude directly from the DAS data. Furthermore, the empirical relation we obtain from one area can also be applied to another new region with slight calibration. Our empirical relation can significantly expand the applications of the DAS technique in earthquake research, such as seismic hazard assessment and earthquake early warning.

1 Introduction

Rapid earthquake source characterization is critical for earthquake monitoring, Earthquake Early Warning (EEW), and prompt reactions to seismic hazards. However, this is still challenging for many remote areas with insufficient seismic station coverage. For example, subduction zones, which can hold the largest earthquakes, are generally poorly instrumented due to the large expenses involved in deploying and maintaining offshore seismic instruments. In this context, Distributed Acoustic Sensing (DAS), which can utilize pre-existing telecommunication fiber-optic cables in both onshore and offshore regions, appears to be a promising complementary sensing method to fill the geographical gaps of conventional seismic networks.

DAS is an emerging technique that has great potential in seismology. It converts every few meters of optical fiber into a single-component strainmeter (Benioff, 1935) to provide spatially coherent signals with high sensitivity. One single DAS array often consists of thousands of channels covering tens of kilometers, and can serve as a dense seismic array to achieve great spatial resolution. DAS has proved to be an effective tool to refine regional seismic structure (Ajo-Franklin et al., 2019; Trainor-Guitton et al., 2019; Yu et al., 2019; Spica, Nishida, et al., 2020; Yang et al., 2022; Spica, Perton, et al., 2020), detect local earthquakes (Ajo-Franklin et al., 2019; Li et al., 2021; Li & Zhan, 2018; Atterholt et al., 2022), and detect seismic signals from various sources (Williams et al., 2019; X. Wang et al., 2020; Zhan et al., 2021; Viens et al., 2022). The phase information of DAS has been well-validated to be accurate in the multiple aforementioned applications. However, DAS nano-strain amplitudes, which commonly represent the direct output from

an interrogator unit, are rarely considered for earthquake source characterization and early-warning purposes.

The direct use of DAS amplitude information is mainly circumscribed by a few limitations such as unknown cable coupling, single-component sensing, uncertain instrumental response, and uncommon amplitude saturation behaviors (Lindsey et al., 2020). DAS instruments record phase shifts of light traveling in the optical fiber and the phase information is then converted into the strain along the cable direction (Lindsey et al., 2017; Fernández-Ruiz et al., 2020; Lindsey & Martin, 2021). However, the instrumental strain is not necessarily equal to the strain of the medium surrounding the cable due to different installation methods of telecommunication cables (Ajo-Franklin et al., 2019). This coupling issue commonly exists but varies with the unknown cable installation in different regions (Ajo-Franklin et al., 2019; Lindsey et al., 2020; Trainor-Guitton et al., 2019; Paitz et al., 2020). Moreover, the instrumental response of DAS is highly frequency-dependent (Lindsey et al., 2020; Paitz et al., 2020) and often hard to quantify without co-located seismometers. The frequency-dependent instrumental response can contaminate frequency components of the DAS data, and may prevent robust spectral analysis. The DAS amplitude saturation is another issue and is sometimes observed for earthquakes close to DAS instruments (Viens et al., 2022). The DAS amplitude saturation is often presented by a flip from maximum to minimum due to the phase wrapping of the sensing laser pulse in the cable (Ajo-Franklin et al., 2022), making this behavior hard to identify and recover. All these instrumental limitations aggravate the accurate conversion of DAS amplitude to ground motions (e.g., velocity and acceleration), thus further challenging the incorporation of DAS data into many seismology applications (Lindsey & Martin, 2021; Farghal et al., 2022). There have been many attempts to convert DAS-recorded strain to ground motions (Daley et al., 2016; H. F. Wang et al., 2018; Yu et al., 2019; Lindsey et al., 2020; Lior et al., 2021). For example, H. F. Wang et al. (2018) showed a good match between DAS amplitude and strain derived from individual co-located nodal sensors. However, Muir and Zhan (2022) systematically reconstructed the strain-rate wavefield with the entire nodal array in the same experiment, and found that the DAS-recorded amplitudes are on average twice that of conventional sensors. In general, accurate conversion requires good knowledge of the local geology, seismic velocity structure, and instrumental information; and is still an active research direction in the DAS community.

Instead of converting DAS-strain data to ground motion measurements (i.e., velocity and acceleration), we propose a data-driven way to explore the relationship between the peak amplitude of DAS data and earthquake magnitude. In this study, we present the first DAS amplitude scaling relation for a rapid magnitude estimation of DAS-recorded earthquakes. Previous studies using conventional strainmeters show that the peak strain amplitude follows an empirical relation that can be used to estimate the earthquake magnitude (Barbour & Crowell, 2017; Barbour et al., 2021). Unlike conventional strainmeters, one DAS array can easily provide thousands of peak amplitude measurements from a single earthquake, allowing the development of robust scaling relation with fewer earthquakes.

We analyze earthquakes recorded by DAS arrays in California, USA, and Sanriku, Japan (Figure 1). Both regions are seismically active and provide us with an unprecedented opportunity to develop and validate the DAS scaling relation. We measure peak DAS amplitudes of earthquakes based on earthquake catalogs. We apply an iterative regression analysis to these datasets to obtain a robust scaling relation between the peak DAS strain rate, earthquake magnitude, and hypocentral distance, calibrated by channel-specific site terms. The obtained scaling relation can then give a rapid but accurate earthquake magnitude estimation from the DAS amplitude measurements. Furthermore, we show that the DAS amplitudes in different regions follow the same scaling relation. The scaling relation built on terrestrial DAS arrays in California can be transferred to the submarine DAS data in Japan. We conclude that our DAS scaling relation is transfer-

122 able for earthquakes within similar distance range, and have great potential in earthquake
 123 source study and EEW.

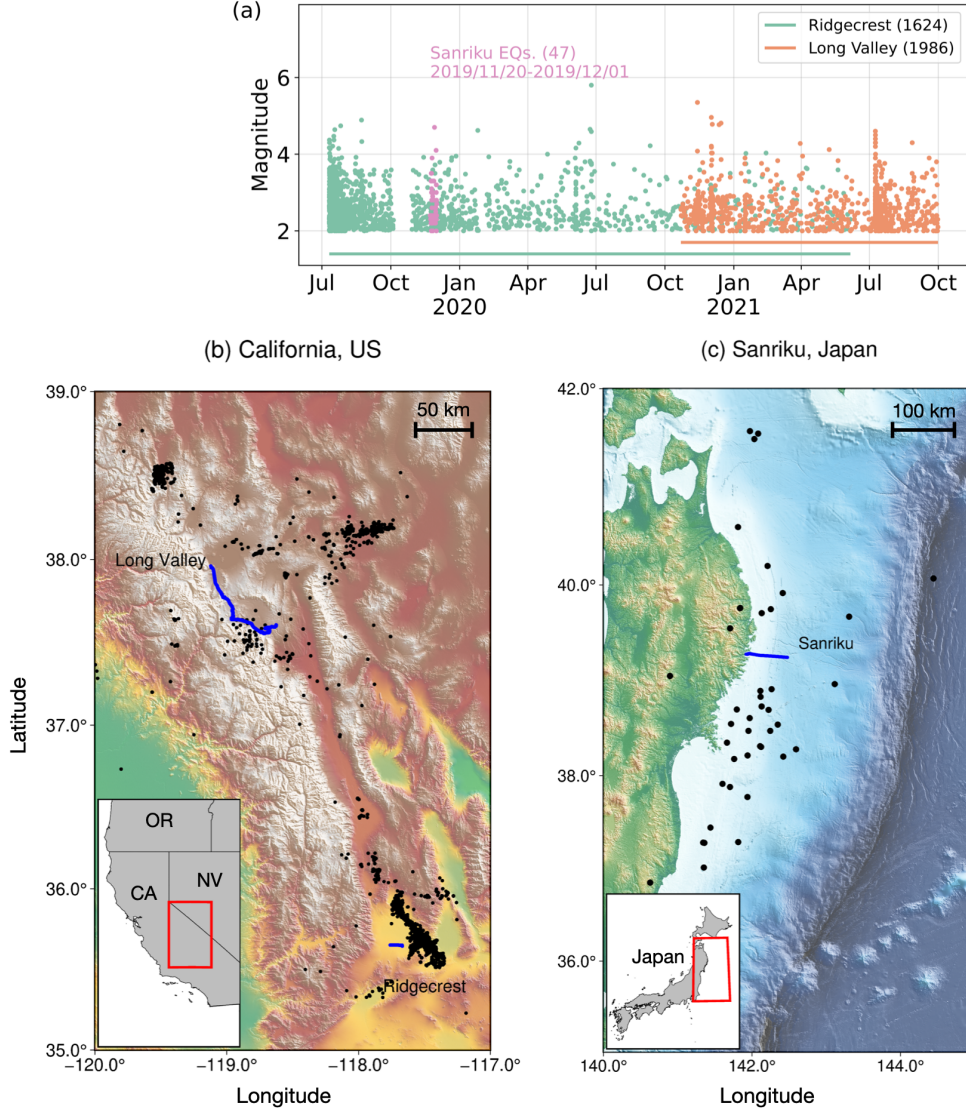


Figure 1. Earthquakes in the study areas. (a) Time variation of earthquakes used in the analysis. Colors indicate earthquakes recorded by different DAS arrays. (b) Topographic map including earthquake locations and the two California DAS arrays: Ridgecrest array and Long-Valley. (c) Map showing the locations of earthquakes and the Sanriku DAS array. Earthquakes are indicated by the black dots and the DAS arrays are shown by blue lines.

2 Results

2.1 Data

We analyze strain-rate DAS data, which is shown to have a frequency-independent instrumental noise (Lior et al., 2022), recorded in both terrestrial and submarine environments (Figure 1 (a)). We start with the two terrestrial DAS arrays in the Ridgecrest (RC) and Long-Valley (LV) regions (Figure 1 (b)) in California. The two arrays recorded over two years of continuous data from July 10, 2019 to October 31, 2021. We first convert the DAS raw data, which is the phase shift of Rayleigh back-scattered laser signals in the optical fiber, to strain rate using Eq. S1 (Text S1 in the Supporting Information). We then apply PhaseNet-DAS (Zhu et al., 2022), which is a deep learning phase picker tailored for DAS data, to accurately pick P-wave and S-wave arrivals from earthquakes (Text S2 of the Supporting Information). We associate the picked earthquakes with the regional earthquake catalogs to determine their locations and magnitudes. We also investigate two weeks of submarine data (November 11, 2019 to December 1, 2019) from a DAS array in Sanriku, Japan (Shinohara et al., 2022). The submarine DAS data suffers from various types of ocean noise and earthquake P-wave arrivals are rarely observed. Due to these limitations, PhaseNet-DAS is not as effective on submarine data as on terrestrial DAS arrays. Instead, we apply a template matching method to detect S-waves from earthquakes, and associate them with the local Japanese Meteorological Agency (JMA) catalog for their location and magnitude (Text S3 of the Supporting Information). In this study, we assume that the difference in catalog magnitude of the two regions, California (local magnitude M_L for most earthquakes or moment magnitude M_w if available) and Sanriku M_{JMA} (velocity magnitude according to JMA (Katsumata, 1996; Funasaki, 2004)), is negligible to simplify the analysis.

We successfully obtain 3,610 earthquakes with 2,363,585 P-wave and 2,411,592 S-wave peak measurements from the two California DAS arrays, and 47 earthquakes with 34,803 S-wave peak measurements from the Sanriku DAS array. The measured peak DAS strain rates present strong correlations with the event magnitude (Figures 2 (c) and (f)) and hypocentral distance (Figures 2 (d) and (g)), respectively. Furthermore, all arrays in different environments follow similar trends and imply the existence of a scaling relation (see Text S4 of the Supporting Information for details of data processing and quality control).

2.2 Scaling relation

Based on the statistical correlations of data (Figure 2), we fit the data with a general form of scaling relation similar to Barbour and Crowell (2017); Barbour et al. (2021):

$$\log_{10} E_i = aM + b\log_{10} D_i + K_i, \quad (1)$$

where E is the observed peak amplitude of DAS strain rate in microstrain/s ($10^{-6}/s$), D is the hypocentral distance in kilometers to each DAS channel and M is the earthquake magnitude. The subscript i corresponds to each DAS channel. We apply a channel-specific factor K_i to account for integrated local effects such as the cable construction, installation, instrumental coupling, and variety of regional geology.

We use an iterative regression method to fit for the magnitude coefficient a , distance coefficient b , and corresponding site terms K_i separately for P and S wave. We first apply it to individual DAS arrays and find that the values are almost the same among various arrays (Figure S1). Therefore, we further combine different data sets for an integrated regression. Because of the unbalanced amount of measurements and different processing steps of terrestrial and submarine DAS data, we separate the two data sets for different purposes. We use the California DAS dataset with both P- and S-wave mea-

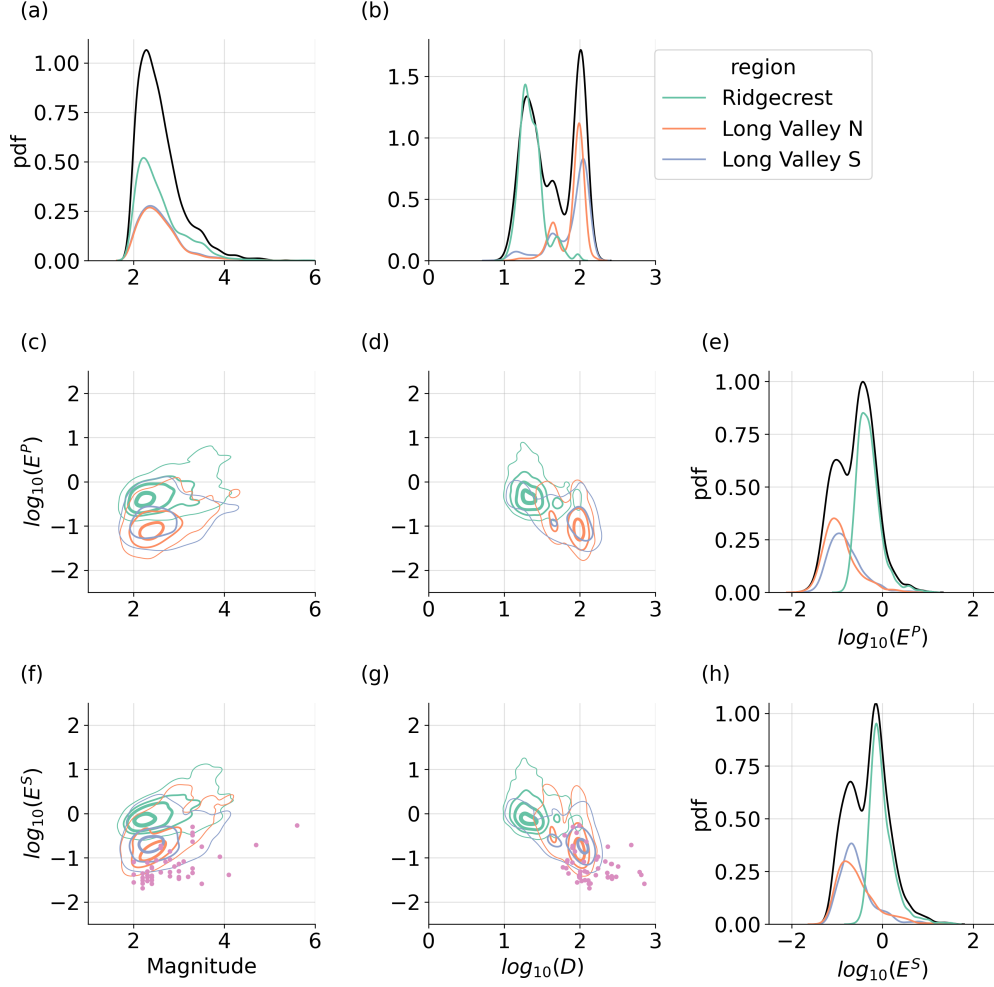


Figure 2. Distributions and correlations of DAS data. (a) Histograms of earthquake magnitude. (b) Histograms of hypocentral distance. (c) Correlation between magnitude and peak P-wave DAS strain rate E^P . (d) Correlation between hypocentral distance and peak P-wave DAS strain rate E^P . (e) Histograms of peak P-wave DAS strain rate E^P . (f) Correlation between magnitude and peak S-wave DAS strain rate E^S . (g) Correlation between hypocentral distance and peak S-wave DAS strain rate E^S . (h) Histograms of peak S-wave DAS strain rate E^S . For histograms, black lines indicate the entire data set of all DAS arrays. Colored lines are for individual arrays. For the 2-D correlation figures, peak DAS strain rate measurements have been averaged by events. Different California arrays are shown by the colored contours, whose levels correspond to 5%, 30%, 60% and 90% of the probability density from thin to thick lines. The Sanriku data points are shown by pink dots on (f) and (g).

surements to fit for the coefficients of Eq.(1), and the Sanriku submarine DAS data as a validation set. This splitting scheme aims at testing the generality of the scaling relation. The best-fit scaling relation we obtain for P waves is:

$$\log_{10} E_i^P = 0.437M - 1.269 \log_{10} D_i + K_i^P, \quad (2)$$

174

and for S waves is:

$$\log_{10} E_i^S = 0.690M - 1.588 \log_{10} D_i + K_i^S. \quad (3)$$

175

We refer the reader to Text S5 and Text S6 of the Supporting Information for further details about the iterative regressions and site calibration terms, respectively.

176

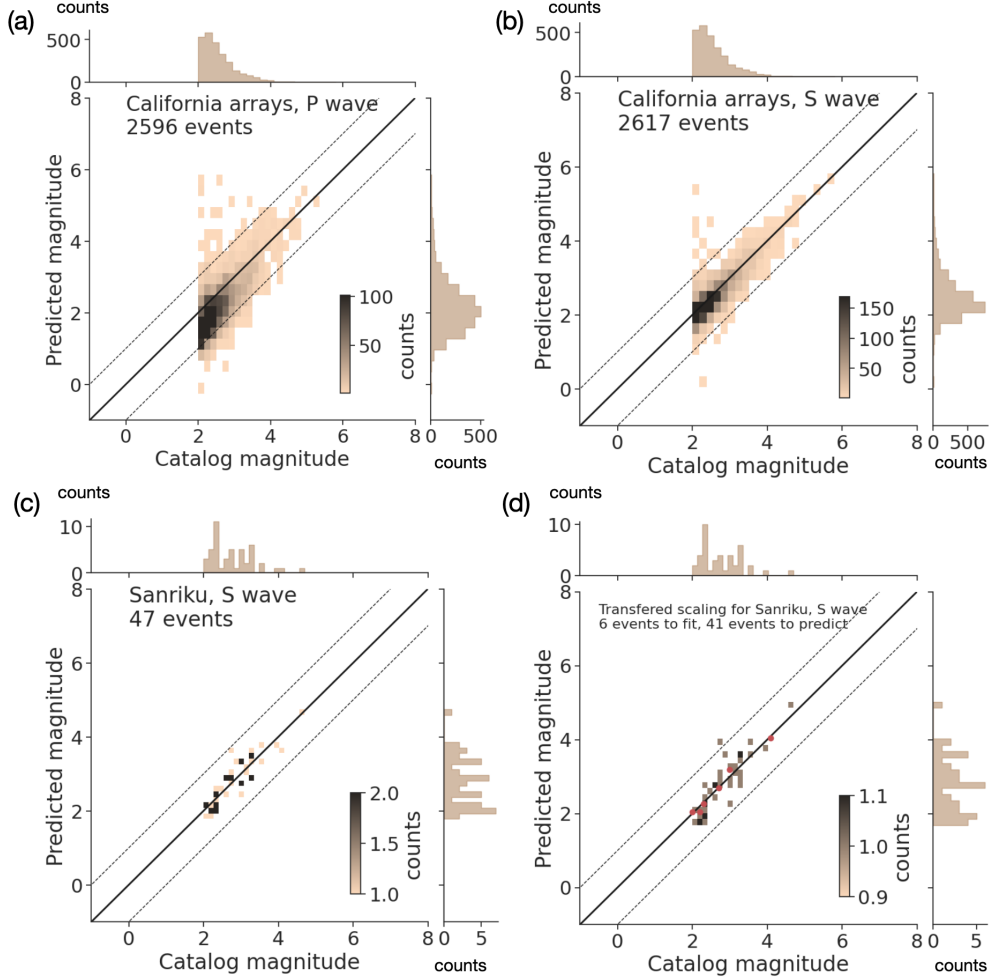


Figure 3. Comparison between earthquake catalog magnitude and magnitude estimated from the scaling relation. (a) Magnitude from the P-wave scaling relation applied to the California data. The scaling relation is from all three California DAS arrays. (b) Magnitude from the S-wave scaling relation applied to the California data. The scaling relation is from all three California DAS arrays. (c) Magnitude from the S-wave scaling relation applied to the Sanriku data. The scaling relation is from the Sanriku DAS array. (d) Magnitude from the S-wave scaling relation applied to the Sanriku data. The scaling relation is transferred from California DAS arrays. Red dots highlight the events used to calibrate the local site terms. Black solid lines indicate the accurate estimation that catalog magnitude is equal to the predicted magnitude. Dashed lines indicate the plus/minus 1 unit of magnitude errors.

2.3 Magnitude estimation from DAS

We validate the scaling relation by comparing the measured peak strain rate with those calculated by the scaling relation Eq.(1) to guarantee that the regression can robustly explain the features in the data (Text S7 and Figure S3 of the Supporting Information). Then, we reorganize the scaling relation Eq.(1) to estimate earthquake magnitudes from the DAS peak strain rate:

$$M_i = (\log_{10} E_i - b \log_{10} D_i - K_i)/a. \quad (4)$$

Given the peak amplitude E_i and hypocentral distance D_i , we calculate the magnitude M_i for each DAS channel and then use the median magnitude of all channels as the final magnitude estimation M . Our results show that the magnitude can be accurately estimated with an error of less than 1 unit of magnitude by using only 2 seconds of either P or S waves (Figure 3 (a)-(c)) for most earthquakes in both the California and Sanriku regions, especially for the larger earthquakes. Moreover, we show that the scaling relation can be transferred from California to Sanriku, and work equally well as that obtained from the Sanriku-only measurements (Figure 3 (d)). The transferred scaling relation inherits the same magnitude a and hypocentral distance b coefficients from the California dataset. They only require a small number of local earthquakes to recalculate the site calibration terms K_i . We apply a systematic random test to show that for the Sanriku case, 6 events are sufficient to get robust values of the site calibration terms (Text S8 of the Supporting Information). The transferred scaling relation can provide an excellent estimation of the magnitude of earthquakes beyond the fitting dataset (Figure 3(d)).

3 Discussion

3.1 Transferable scaling relation of DAS amplitude

Unlike conventional seismic sensors, DAS instruments are commonly deployed on preexisting telecommunication optical fibers with various properties and construction designs (Ajo-Franklin et al., 2019). These differences lead to difficulties in determining the instrument responses of DAS arrays. Some previous studies have shown that DAS instrument responses can be quantitatively determined by comparing DAS measurements with a co-located seismometer (Lindsey et al., 2020; Paitz et al., 2020), which is not always available, especially in marine environments. There are multiple ways to convert DAS measurements to ground motions: for instance, direct calibration with co-located seismometers (Lindsey et al., 2017); correction based on apparent local phase velocity (Daley et al., 2016; H. F. Wang et al., 2018; Yu et al., 2019; Shinohara et al., 2022); spatial integration from one co-located seismometer (H. F. Wang et al., 2018); rescaling in the $f-k$ or curvelet domains (Lindsey et al., 2020; Yang et al., 2022). Although shown to be effective, most of these methods require elaborate data preprocessing and analyst-intensive quality control, making them cable-dependent and thus limiting the applications of DAS in different regions and for real-time operations.

In this study, we evaluate how DAS amplitude is related to earthquake magnitude in a data-driven methodology. With the abundant peak amplitude measurements of earthquakes in the Ridgecrest and Long-Valley regions, we apply the regression analysis to obtain a robust scaling relation for both P- and S-waves recorded by DAS instruments. Most importantly, we find that different regions have almost the same values of the scaling coefficients a and b (Figure S1) with regional site calibration terms K_i (Figures S2 and S4 in the Supporting Information). Our results show that the scaling relation can be transferred/extrapolated from one well-studied area to other DAS arrays for earthquakes within a similar distance range. The DAS peak amplitude scaling relation can be applied to earthquake source studies in different areas.

We further compare the DAS measurements with results from previous studies using conventional strainmeters (Barbour et al., 2021). The distance coefficients of both conventional strainmeters and DAS are close, meaning that the dynamic strain follows the same geometrical spreading of wave propagation for both conventional strainmeters and DAS instruments. However, the magnitude coefficients are different mainly because the DAS scaling relation is built based on strain rate, while the scaling relation of conventional strainmeters are built based on strain. The different physical quantities scale differently with earthquake magnitude. Strain rate is theoretically proportional to acceleration (Benioff, 1935). Therefore, we analyze the peak ground acceleration (PGA) of the Next Generation Attenuation model (NGA-West2) project (Bozorgnia et al., 2014). For consistent comparisons, we fit the PGA dataset with the same model as Eq.1, assigning the site calibration term to each station. We find that the distance coefficients from DAS are close to those from PGA (Figure S1). Differences in the magnitude coefficients are probably due to the different frequency bands of DAS and conventional accelerometers. Nowadays, Ground Motion Prediction Equations (GMPEs) with many parameters have been developed from various datasets to predict earthquake ground motions for engineering and seismological applications (Zhao et al., 2006; Kanno et al., 2006; Boore & Atkinson, 2008; Bozorgnia et al., 2014; Boore et al., 2014; Campbell & Bozorgnia, 2014). Modern GMPEs have detailed definitions of the distance dependence (geometrical and inelastic attenuation) and local site responses (local geology, seismic structure, instrument deployment, etc.) to explain the ground motion data in different regions. Because of the relatively early stages of the DAS technique and limited data from different locations, we decide to start with the simplest form of scaling relation as Eq.1 in this study for a first-order validation of the DAS scaling relation. We leave more complex DAS strain prediction equations for future studies.

3.2 Potential applications of the DAS scaling relation

Our peak DAS amplitude scaling relation is fundamental and significant for various seismological studies such as earthquake seismology and EEW. Regarding earthquake source analyses using DAS, the current studies only focus on earthquake detection and location using the time information (Lindsey et al., 2017; Lellouch et al., 2020; Li et al., 2021; Yang et al., 2022; Atterholt et al., 2022; Viens et al., 2022). Adding the amplitude information and constraints on the earthquake magnitude can significantly help us to resolve more source parameters and physical details about the earthquake rupture.

Another substantial application is for EEW, which has shown to be an effective method to mitigate seismic risk. EEW aims to rapidly estimate the ground motion from real-time data after an earthquake occurs and sends out alerts to specific users and the public (Allen & Melgar, 2019). Current EEW algorithms use conventional seismic data for ground motion predictions. As DAS leverages pre-existing telecommunication fiber-optic cables, it can complement the current EEW systems. Converting most telecommunication cables located in highly seismic active regions into dense arrays of sensors could provide an economical approach to extend and improve the current EEW system, especially in offshore seismogenic zones.

A recent study has attempted to apply DAS in EEW (Lior et al., 2022). Their application relies on accurate conversion from DAS strain rate to ground acceleration, which is used for earthquake magnitude estimation and ground motion prediction (Lior et al., 2021). Our scaling relation provide an alternative and new approach to obtain earthquake magnitude from DAS measurements. Compared with conversion-based methods, there are a few advantages in using data-driven scaling relation of DAS measurements. Firstly, the scaling relation is built upon abundant direct DAS measurements, and they do not require an intensive manual pre-processing or parameter tuning, simplifying the deployment on edge-computing (Shi et al., 2016). Secondly, the scaling relation accounts for the different coupling and regional effects among DAS channels with the site calibration

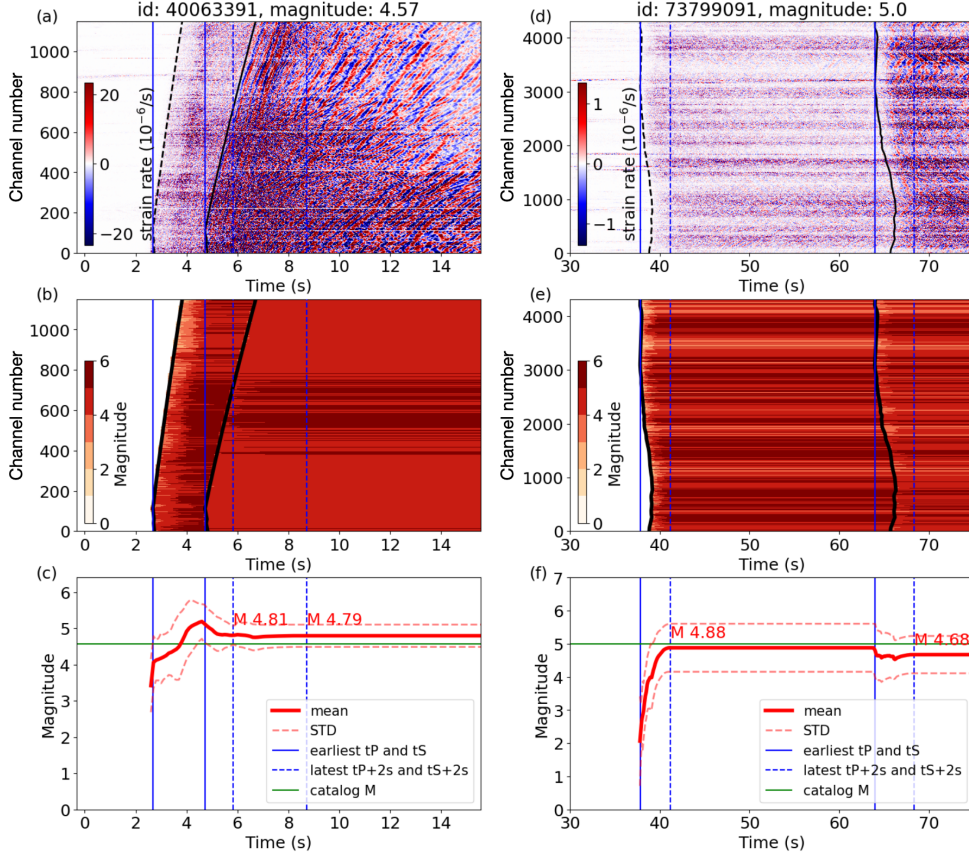


Figure 4. Idealized real-time earthquake magnitude estimation with the scaling relation. (a) Streaming DAS data from an M4.57 earthquake that occurred in Ridgecrest region. The initial time of earthquake is set as 0 second. (b) The corresponding magnitude estimation based on the peak DAS amplitude for each channel. The black lines indicate the arrival of the P-wave and the S-wave. (c) The final magnitude estimation from averaging magnitude estimation at all available channels, shown by the red line. The red dashed lines indicate the standard deviation of magnitude estimation from channels. The green horizontal lines indicate the catalog magnitude. The blue vertical lines show the earliest P- and S- arrivals, respectively. The blue vertical dashed lines show 2 seconds after the latest P- and S- arrivals, respectively. (d)-(f) show results of another M5.0 earthquake recorded by Long Valley north array.

terms, and no manual identification of well-coupled fiber is required. Last but not least, as demonstrated in the example of Sanriku results, the scaling relation is transferable. We can easily transfer the scaling relation from one well-studied region to other regions for deployment of new systems. Only a small number of earthquakes are required to calibrate the site terms. Then, the scaling relation can be promptly employed for rapid earthquake magnitude estimation in a new region. Technically, the regional scaling relation can also be consistently updated with more regional measurements of earthquakes.

Finally, we conduct an idealized experiment to illustrate the potential application of the DAS scaling relation for rapid magnitude estimation. We assume that the earthquake can be immediately detected and located. Therefore, we can apply the scaling relation to convert the streaming DAS signals (Figure 4 (a) and (d)) to real-time estima-

tion of earthquake magnitude (Figure 4 (b) and (e)) at available DAS channels. We keep the median value of magnitude estimated at each channel as the final estimation and keep updating it with time (Figure 4 (c) and (f)). We experiment with the recent M4.57 and M5.0 earthquakes recorded by the Ridgecrest and Long-Valley north arrays, respectively. The M4.57 earthquake occurred on July 15, 2022 in the Ridgecrest region and is about 15 km from the Ridgecrest array. The M5.0 earthquake occurred on October 25, 2022, near Alum Rock and San Jose, California and is about 244 km from the Long Valley array. Both events are not included in the data sets that are used for the regression, and therefore are good candidates to test our scaling relation on earthquakes from different distance. We can accurately estimate the event magnitude with its uncertainty less than 0.5 only 2 seconds after the earliest P-wave arrival. When some channels begin to detect the S wave, we also include the S wave information by averaging the magnitude from both P-wave and S-wave amplitudes to further update the magnitude estimation. It is also possible to combine rapid estimation of earthquake magnitude with the GMPEs (Atkinson & Boore, 2006; Boore & Atkinson, 2008; Bozorgnia et al., 2014; Douglas & Edwards, 2016) to predict the ground shaking and seismic intensity, similar to the conventional EEW systems based on earthquake point source modeling (Allen & Melgar, 2019). More details about the method are provided in Section 9.

However, this data-driven scaling analysis method also has some limitations that require further studies. The scaling relation of peak DAS amplitude relies on correct event association and peak amplitude measurement. Measurement of peak amplitude in the improper waveform window can lead to errors in the magnitude estimation. For instance, there are a few small events with largely overestimated magnitudes in our results (Figures 3(a)-(b)). We investigate the waveforms of those events and find that the overestimation is due to an incorrect event association. For instance, an M2 event in the Long-Valley region is estimated as an M6 earthquake, because this event is a foreshock occurring only 8 seconds before the M6.0 earthquake. We also find a few instances where multiple events occur in different places but are recorded at the same time, leading to overlapped arrivals in the same time window. In such cases, the peak amplitudes of weaker arrivals will be overestimated. Combining DAS with other independent seismic sensors can help to exclude the incorrectly associated event, thus improving the magnitude estimation. Finally, our current datasets only contain moderate magnitude earthquakes ($M < 6$) due to the short period of DAS deployment. Future DAS campaigns focusing on EEW and recording large earthquakes should explore if the scaling relation still holds or behaves differently due to potential complex non-linear site response (Bonilla et al., 2011; Astorga et al., 2018; Viens et al., 2022).

4 Conclusion

This work presents the first scaling relation between DAS peak amplitude, earthquake magnitude, and hypocentral distance from terrestrial and submarine DAS arrays. We show that we could use the scaling relation to rapidly estimate the magnitude of earthquakes in near real time. Furthermore, we find that the scaling relation is transferable from terrestrial DAS arrays in California to a submarine DAS array in Sanriku, Japan. Our results indicate a possibly universal scaling relation for DAS recorded peak amplitudes. The DAS amplitude scaling relation has great potential in different seismological studies such as EEW and earthquake source characterization.

Acknowledgments

The authors would like to thank Jessie Saunders at California Institute of Technology and Richard Allen at University of California, Berkeley for their constructive suggestions. This work was supported by Office of Emergency Services, State of California, under MCG.CEEWS3-1-CALIFOES.NEWS, funding source award number 6113-2019. YM and LV were sup-

ported by NSF award EAR2022716. This article has a Los Alamos National Laboratory (LANL) Unlimited Release Number (LA-UR-23-20408).

Data Availability Statement

The measured peak strain rate amplitude from multiple DAS arrays is available from the Caltech DATA repository with the link in a separate supplement document. This is temporarily used for the reviewers and will become publicly available upon publication. The Python scripts to process the data and reproduce results are available at https://github.com/yinjiuxun/das_strain_scaling.

References

- Ajo-Franklin, J. B., Dou, S., Lindsey, N. J., Monga, I., Tracy, C., Robertson, M., ... Li, X. (2019). Distributed acoustic sensing using dark fiber for near-surface characterization and broadband seismic event detection. *Scientific Reports*, 9(1), 1328. doi: 10.1038/s41598-018-36675-8
- Ajo-Franklin, J., Rodríguez Tribaldos, V., Nayak, A., Cheng, F., Mellors, R., Chi, B., ... Dobson, P. (2022). The imperial valley dark fiber project: Toward seismic studies using das and telecom infrastructure for geothermal applications. *Seismological Research Letters*. doi: 10.1785/0220220072
- Allen, R. M., & Melgar, D. (2019). Earthquake early warning: Advances, scientific challenges, and societal needs. *Annual Review of Earth and Planetary Sciences*, 47(1), 361–388. doi: 10.1146/annurev-earth-053018-060457
- Astorga, A., Guéguen, P., & Kashima, T. (2018). Nonlinear elasticity observed in buildings during a long sequence of earthquakes. *Bulletin of the Seismological Society of America*, 108(3A), 1185–1198.
- Atkinson, G. M., & Boore, D. M. (2006). Earthquake ground-motion prediction equations for eastern north america. *Bulletin of the Seismological Society of America*, 96(6), 2181–2205. doi: 10.1785/0120050245
- Atterholt, J., Zhan, Z., Shen, Z., & Li, Z. (2022). A unified wavefield-partitioning approach for distributed acoustic sensing. *Geophysical Journal International*, 228(2), 1410–1418. doi: 10.1093/gji/ggab407
- Barbour, A. J., & Crowell, B. W. (2017). Dynamic strains for earthquake source characterization. *Seismological Research Letters*, 88(2), 354–370. doi: 10.1785/0220160155
- Barbour, A. J., Langbein, J. O., & Farghal, N. S. (2021). Earthquake magnitudes from dynamic strain. *Bulletin of the Seismological Society of America*, 111(3), 1325–1346. doi: 10.1785/0120200360
- Benioff, H. (1935). A linear strain seismograph. *Bulletin of the Seismological Society of America*, 25(4), 283–309.
- Bonilla, L. F., Tsuda, K., Pulido, N., Régnier, J., & Laurendeau, A. (2011). Non-linear site response evidence of k-net and kik-net records from the 2011 off the pacific coast of tohoku earthquake. *Earth, planets and space*, 63(7), 785–789.
- Boore, D. M., & Atkinson, G. M. (2008). Ground-motion prediction equations for the average horizontal component of pga, pgv, and 5periods between 0.01 s and 10.0 s. *Earthquake Spectra*, 24(1), 99–138. doi: 10.1193/1.2830434
- Boore, D. M., Stewart, J. P., Seyhan, E., & Atkinson, G. M. (2014). Nga-west2 equations for predicting pga, pgv, and 5earthquakes. *Earthquake Spectra*, 30(3), 1057–1085. doi: 10.1193/070113EQS184M
- Bozorgnia, Y., Abrahamson, N. A., Atik, L. A., Ancheta, T. D., Atkinson, G. M., Baker, J. W., ... Youngs, R. (2014). Nga-west2 research project. *Earthquake Spectra*, 30(3), 973–987. doi: 10.1193/072113EQS209M
- Campbell, K. W., & Bozorgnia, Y. (2014). Nga-west2 ground motion model for the average horizontal components of pga, pgv, and 5% damped linear ac-

- celeration response spectra. *Earthquake Spectra*, 30(3), 1087–1115. doi: 10.1193/062913EQS175M
- Daley, T. M., Miller, D. E., Dodds, K., Cook, P., & Freifeld, B. M. (2016). Field testing of modular borehole monitoring with simultaneous distributed acoustic sensing and geophone vertical seismic profiles at Citronelle, Alabama. *Geophysical Prospecting*, 64(5), 1318–1334. doi: 10.1111/1365-2478.12324
- Douglas, J., & Edwards, B. (2016). Recent and future developments in earthquake ground motion estimation. *Earth-Science Reviews*, 160, 203–219. doi: 10.1016/j.earscirev.2016.07.005
- Farghal, N. S., Saunders, J. K., & Parker, G. A. (2022). The potential of using fiber optic distributed acoustic sensing (das) in earthquake early warning applications. *Bulletin of the Seismological Society of America*. doi: 10.1785/0120210214
- Fernández-Ruiz, M. R., Soto, M. A., Williams, E. F., Martín-López, S., Zhan, Z., González-Herrera, M., & Martins, H. F. (2020). Distributed acoustic sensing for seismic activity monitoring. *APL Photonics*, 5(3), 030901. doi: 10.1063/1.5139602
- Funasaki, J. (2004). Revision of the jma velocity magnitude. *Quart. J. Seismol.*, 67, 11–20.
- Kanno, T., Narita, A., Morikawa, N., Fujiwara, H., & Fukushima, Y. (2006). A new attenuation relation for strong ground motion in Japan based on recorded data. *Bulletin of the Seismological Society of America*, 96(3), 879–897. doi: 10.1785/0120050138
- Katsumata, A. (1996). Comparison of magnitudes estimated by the Japan Meteorological Agency with moment magnitudes for intermediate and deep earthquakes. *Bulletin of the Seismological Society of America*, 86(3), 832–842.
- Lellouch, A., Lindsey, N. J., Ellsworth, W. L., & Biondi, B. L. (2020). Comparison between distributed acoustic sensing and geophones: Downhole microseismic monitoring of the Forge geothermal experiment. *Seismological Research Letters*, 91(6), 3256–3268. doi: 10.1785/0220200149
- Li, Z., Shen, Z., Yang, Y., Williams, E., Wang, X., & Zhan, Z. (2021). Rapid response to the 2019 Ridgecrest earthquake with distributed acoustic sensing. *AGU Advances*, 2(2), e2021AV000395. doi: 10.1029/2021AV000395
- Li, Z., & Zhan, Z. (2018). Pushing the limit of earthquake detection with distributed acoustic sensing and template matching: A case study at the Brady geothermal field. *Geophysical Journal International*, 215(3), 1583–1593. doi: 10.1093/gji/ggy359
- Lindsey, N. J., & Martin, E. R. (2021). Fiber-optic seismology. *Annual Review of Earth and Planetary Sciences*, 49(1), 309–336. doi: 10.1146/annurev-earth-072420-065213
- Lindsey, N. J., Martin, E. R., Dreger, D. S., Freifeld, B., Cole, S., James, S. R., ... Ajo-Franklin, J. B. (2017). Fiber-optic network observations of earthquake wavefields. *Geophysical Research Letters*, 44(23), 11,792–11,799. doi: 10.1002/2017GL075722
- Lindsey, N. J., Rademacher, H., & Ajo-Franklin, J. B. (2020). On the broadband instrument response of fiber-optic das arrays. *Journal of Geophysical Research: Solid Earth*, 125(2), e2019JB018145. doi: 10.1029/2019JB018145
- Lior, I., Rivet, D., Ampuero, J. P., Sladen, A., Barrientos, S., Sánchez-Olavarria, R., ... Prado, J. A. B. (2022). Harnessing distributed acoustic sensing for earthquake early warning: Magnitude estimation and ground motion prediction.
- Lior, I., Sladen, A., Mercier, D., Ampuero, J.-P., Rivet, D., & Sambolian, S. (2021). Strain to ground motion conversion of distributed acoustic sensing data for earthquake magnitude and stress drop determination. *Solid Earth*, 12(6), 1421–1442. doi: 10.5194/se-12-1421-2021
- Muir, J. B., & Zhan, Z. (2022). Wavefield-based evaluation of das instrument re-

- sponse and array design. *Geophysical Journal International*, 229(1), 21–34. doi: 10.1093/gji/ggab439
- Paitz, P., Edme, P., Gräff, D., Walter, F., Doetsch, J., Chalari, A., . . . Fichtner, A. (2020). Empirical investigations of the instrument response for distributed acoustic sensing (das) across 17 octaves. *Bulletin of the Seismological Society of America*, 111(1), 1–10. doi: 10.1785/0120200185
- Shi, W., Cao, J., Zhang, Q., Li, Y., & Xu, L. (2016). Edge computing: Vision and challenges. *IEEE internet of things journal*, 3(5), 637–646.
- Shinohara, M., Yamada, T., Akuhara, T., Mochizuki, K., & Sakai, S. (2022). Performance of seismic observation by distributed acoustic sensing technology using a seafloor cable off sanriku, japan. *Frontiers in Marine Science*, 466.
- Spica, Z. J., Nishida, K., Akuhara, T., Pétrélis, F., Shinohara, M., & Yamada, T. (2020). Marine sediment characterized by ocean-bottom fiber-optic seismology. *Geophysical Research Letters*, 47(16), e2020GL088360. doi: 10.1029/2020GL088360
- Spica, Z. J., Perton, M., Martin, E. R., Beroza, G. C., & Biondi, B. (2020). Urban seismic site characterization by fiber-optic seismology. *Journal of Geophysical Research: Solid Earth*, 125(3), e2019JB018656. doi: 10.1029/2019JB018656
- Trainor-Guitton, W., Guitton, A., Jreij, S., Powers, H., & Sullivan, B. (2019). 3d imaging of geothermal faults from a vertical das fiber at brady hot spring, nv usa. *Energies*, 12(7), 1401. doi: 10.3390/en12071401
- Viens, L., Bonilla, L. F., Spica, Z. J., Nishida, K., Yamada, T., & Shinohara, M. (2022). Nonlinear earthquake response of marine sediments with distributed acoustic sensing. *Geophysical Research Letters*, 49(21), e2022GL100122. doi: 10.1029/2022GL100122
- Wang, H. F., Zeng, X., Miller, D. E., Fratta, D., Feigl, K. L., Thurber, C. H., & Mellors, R. J. (2018). Ground motion response to an ml 4.3 earthquake using co-located distributed acoustic sensing and seismometer arrays. *Geophysical Journal International*, 213(3), 2020–2036. doi: 10.1093/gji/ggy102
- Wang, X., Williams, E. F., Karrenbach, M., Herráez, M. G., Martins, H. F., & Zhan, Z. (2020). Rose parade seismology: Signatures of floats and bands on optical fiber. *Seismological Research Letters*, 91(4), 2395–2398. doi: 10.1785/0220200091
- Williams, E. F., Fernández-Ruiz, M. R., Magalhaes, R., Vanthillo, R., Zhan, Z., González-Herráez, M., & Martins, H. F. (2019). Distributed sensing of micro-seisms and teleseisms with submarine dark fibers. *Nature Communications*, 10(1), 5778. doi: 10.1038/s41467-019-13262-7
- Yang, Y., Atterholt, J. W., Shen, Z., Muir, J. B., Williams, E. F., & Zhan, Z. (2022). Sub-kilometer correlation between near-surface structure and ground motion measured with distributed acoustic sensing. *Geophysical Research Letters*, 49(1), e2021GL096503. doi: 10.1029/2021GL096503
- Yu, C., Zhan, Z., Lindsey, N. J., Ajo-Franklin, J. B., & Robertson, M. (2019). The potential of das in teleseismic studies: Insights from the goldstone experiment. *Geophysical Research Letters*, 46(3), 1320–1328. doi: 10.1029/2018GL081195
- Zhan, Z., Cantono, M., Kamalov, V., Mecozzi, A., Müller, R., Yin, S., & Castellanios, J. C. (2021). Optical polarization-based seismic and water wave sensing on transoceanic cables. *Science*. doi: 10.1126/science.abe6648
- Zhao, J. X., Zhang, J., Asano, A., Ohno, Y., Oouchi, T., Takahashi, T., . . . Fukushima, Y. (2006). Attenuation relations of strong ground motion in japan using site classification based on predominant period. *Bulletin of the Seismological Society of America*, 96(3), 898–913. doi: 10.1785/0120050122
- Zhu, W., Biondi, E., Ross, Z. E., & Zhongwen, Z. (2022). Seismic arrival-time picking on distributed acoustic sensing data using semi-supervised learning. *arXiv preprint*.